Inorganic Chemistry

Article

pubs.acs.org/IC

Influence of the Cation Size on the Framework Structures and Space Group Centricities in $AMo_2O_5(SeO_3)_2$ (A = Sr, Pb, and Ba)

Seung-Jin Oh, Dong Woo Lee, and Kang Min Ok*

Department of Chemistry, Chung-Ang University, 221 Heukseok-dong, Dongjak-gu, Seoul 156-756, Republic of Korea

Supporting Information

ABSTRACT: Two new quaternary mixed-metal selenites, $SrMo_2O_5(SeO_3)_2$ and $PbMo_2O_5(SeO_3)_2$, have been synthesized as crystals and pure polycrystalline phases by standard solid-state reactions using $SrMoO_4$, PbO, MoO_3, and SeO_2 as reagents. The crystal structures of the reported materials have been determined by single-crystal X-ray diffraction. $SrMo_2O_5(SeO_3)_2$ and $PbMo_2O_5(SeO_3)_2$ are isostructural and crystallized in the triclinic centrosymmetric space group $P\bar{1}$ (No. 2). The reported materials exhibit chain structures consisting of MoO_6 octahedra and asymmetric SeO_3 polyhedra. Complete characterizations including IR spectroscopy and thermal analyses for the compounds are also presented, as are dipole moment calculations. In addition, the powder second-harmonic-generating (SHG) properties of noncentrosymmetric polar $BaMo_2O_5(SeO_3)_2$ have been measured using 1064 nm radiation. Through powder SHG measurement, we are able to determine that $BaMo_2O_5(SeO_3)_2$ has a SHG efficiency of approximately 80 times that of α-SiO_2. Additional SHG measurements reveal that the material is phase-matchable (type 1). A detailed cation size effect on the symmetry and framework structure is discussed.

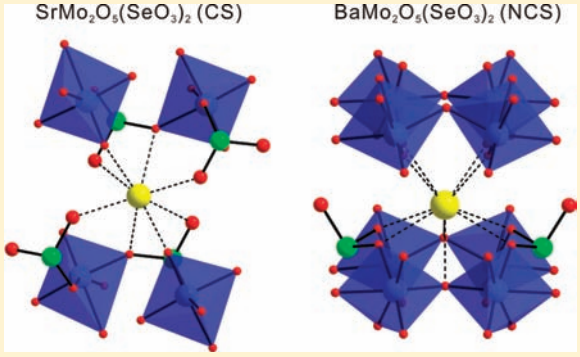

INTRODUCTION

The demand for advanced new functional materials containing noncentrosymmetric (NCS) crystal structures remains very strong because the NCS materials exhibit technologically important properties such as second-order nonlinear optical (NLO), piezoelectric, pyroelectric, and ferroelectric properties.[1−5] Although the relationships between the NCS structures and the above-mentioned properties are well established,[6−8] the development of strategies for rationally designed superior performing NCS materials is still challenging. Thus far, one of the most successful strategies to increasing the crystallographic NCS behavior is introducing cations with asymmetric coordination environments and larger polarizability to the framework structures. With oxide materials, significant numbers of NCS crystal structures have been observed in materials containing cations susceptible to second-order Jahn−Teller (SOJT) distortions.[9−12] SOJT distortions exhibiting asymmetric coordination environments are normally found in two families of cations: octahedrally coordinated d^0 transition metals (Ti^{4+}, V^{5+}, Mo^{6+}, etc.) and cations with stereoactive lone pairs (Sb^{3+}, Se^{4+}, I^{5+}, etc.). In addition, d^{10} transition-metal cations showing polar displacement in the center of the coordination environment, and asymmetric π-orbital systems found in the borate groups are another example of important NCS chromophores.[13,14] All of the local acentricities are necessary but not sufficient for generating NCS because the local asymmetric units often align in an antiparallel manner and crystallize in a centrosymmetric (CS) structure. Thus, it is more important to understand factors determining the space group symmetry to increase the incidence of crystallographic NCS in any new material.[15−18] In fact, there are several reports exhibiting factors that influence the overall centricity, in which the size of the alkali-metal cations and the hydrogen-bonding effect played very important roles.[19−22] With these ideas in mind, we decided to investigate the A^{2+}−Mo^{6+}−Se^{4+}−oxide system. As SOJT-distortive cations, both Mo^{6+} and Se^{4+} cations exhibit highly asymmetric coordination environments. Mo^{6+} has been known to be located at the highest magnitude of the out-of-center distortion scale.[23] Also, Se^{4+} inherently possesses asymmetric structural geometry attributable to the nonbonded electron pair. In fact, several molybdenum selenite materials such as $A_2(MoO_3)_2(SeO_3)$ (A = NH_4, Ag, Rb, Tl, and Cs),[24−26] $BaMoO_3SeO_3$,[27] $Ba(Mo_2O_5)(SeO_3)_2$,[27] A_2MoSeO_6 (A = Na, K, and Rb),[28] $A_2MoSe_2O_{10}$ (A = Nd or Ga),[29,30] $A_2MoSe_3O_{12}$ (A = Gd or Bi),[29,31] $Ni_3(Mo_2O_8)(SeO_3)$,[32] and $Cu_2(MoO_4)(SeO_3)$[33] have been reported. Here we report solid-state syntheses and characterizations of a series of quaternary mixed-metal selenites, $AMo_2O_5(SeO_3)_2$ (A = Sr, Pb, and Ba). We will demonstrate that the cation size and coordination number influence the framework architecture and the space group symmetry of the materials. With the NCS $BaMo_2O_5(SeO_3)_2$, detailed second-harmonic-generating (SHG) properties will also be reported.

Received: February 17, 2012
Published: April 18, 2012

   dx.doi.org/10.1021/ic3003564 | Inorg. Chem. 2012, 51, 5393−5399

EXPERIMENTAL SECTION

Reagents. PbO (Junsei, 99%), $SrCO_3$ (Aldrich, 99.9%), $BaCO_3$ (Duksan, 99.5%), MoO_3 (Hayashi, 99.5%), and SeO_2 (Aldrich, 98%) were used as received. $SrMoO_4$ and $BaMoO_4$ were synthesized by standard solid-state reactions. A stoichiometric amount of $SrCO_3$ (or $BaCO_3$) and MoO_3 was thoroughly ground and pressed into a pellet. The pellet was heated to 600 °C for 24 h and cooled to room temperature. The phase purities of $SrMoO_4$ and $BaMoO_4$ were confirmed by powder X-ray diffraction (XRD).

Synthesis. Crystals of $SrMo_2O_5(SeO_3)_2$ and $PbMo_2O_5(SeO_3)_2$ were prepared by standard solid-state reactions. For single crystals of $PbMo_2O_5(SeO_3)_2$, 0.335 g (1.50×10^{-3} mol) of PbO, 0.432 g (3.00×10^{-3} mol) of MoO_3, and 0.366 g (3.30×10^{-3} mol) of SeO_2 were thoroughly mixed with an agate mortar and pestle and pressed into a pellet. The pellet was introduced into a fused-silica tube, which was subsequently evacuated and sealed. The tube was gradually heated to 400 °C for 36 h and cooled at a rate of 12 °C h^{-1} to room temperature. The product contained colorless block-shaped crystals (60% yield) with white polycrystalline $PbMo_2O_5(SeO_3)_2$. The crystal growth conditions such as the starting reagents and reaction temperature for $SrMo_2O_5(SeO_3)_2$ are slightly different. A total of 0.371 g (1.50×10^{-3} mol) of $SrMoO_4$ and 0.333 g (3.00×10^{-3} mol) of SeO_2 were thoroughly mixed with an agate mortar and pestle and pressed into a pellet. The pellet was transferred to a fused-silica tube, which was evacuated and sealed. The tube was heated to 500 °C for 24 h and then cooled slowly at a rate of 6 °C h^{-1} to 300 °C before being quenched to room temperature. Colorless block-shaped crystals (31% yield) of $SrMo_2O_5(SeO_3)_2$ were recovered with some unknown polycrystalline materials. Pure polycrystalline samples of $AMo_2O_5(SeO_3)_2$ (A = Sr and Ba) were obtained through similar solid-state reactions. A total of 0.495 g (2.00×10^{-3} mol) of $SrMoO_4$ (0.595 g for $BaMoO_4$), 0.288 g (2.00×10^{-3} mol) of MoO_3, and 0.488 g (4.40×10^{-3} mol) of SeO_2 were thoroughly mixed and introduced into a fused-silica tube, and the tube was evacuated and sealed. However, the tube was heated to 400 °C for 36 h. It should also be noted that a 10% excess amount of SeO_2 has been used initially in order to synthesize pure polycrystalline phases of $AMo_2O_5(SeO_3)_2$ attributable to the easy sublimation of SeO_2 at lower temperature. The powder XRD patterns on the resultant polycrystalline products showed that the materials were single phases and were in good agreement with the generated patterns from the single-crystal data (see the Supporting Information).

Single-Crystal XRD. The structures of $SrMo_2O_5(SeO_3)_2$ and $PbMo_2O_5(SeO_3)_2$ were determined by standard crystallographic methods. Colorless block crystals [0.023 × 0.027 × 0.072 mm^3 for $SrMo_2O_5(SeO_3)_2$ and 0.023 × 0.040 × 0.067 mm^3 for $PbMo_2O_5(SeO_3)_2$] were used for single-crystal data analyses. All of the data were collected using a Bruker SMART BREEZE diffractometer equipped with a 1K CCD area detector using graphite-monochromated Mo Kα radiation at 200 K. A hemisphere of data was collected using a narrow-frame method with a scan width of 0.30° in ω and an exposure time of 5 s $frame^{-1}$. The first 50 frames were remeasured at the end of the data collection to monitor the instrument and crystal stability. The maximum correction applied to the intensities was <1%. The data were integrated using the *SAINT* program,[34] with the intensities corrected for Lorentz factor, polarization, air absorption, and absorption attributable to variation of the path length through the detector faceplate. A semiempirical absorption correction was made on the hemisphere of data with the *SADABS* program.[35] The data were solved and refined using *SHELXS-97* and *SHELXL-97*, respectively.[36,37] All calculations were performed using the *WinGX-98* crystallographic software package.[38] Crystallographic data and selected bond distances for the reported material are given in Tables 1 and 2.

Powder XRD. Powder XRD was used to confirm the phase purity for the synthesized materials. The powder XRD pattern was collected on a Bruker D8-Advance diffractometer using Cu Kα radiation at room temperature with 40 kV and 40 mA. The polycrystalline samples were mounted on sample holders and scanned in the 2θ range 5−70° with a step size of 0.02° and a step time of 0.2 s. The experimental powder XRD pattern is in good agreement with the calculated data from the single-crystal model. Because the crystal structure of $BaMo_2O_5(SeO_3)_2$ has been published,[27] the diffraction pattern of $BaMo_2O_5(SeO_3)_2$ was analyzed using the Rietveld method with the *GSAS* program.[39] The 2θ range was 10−100° with a step size of 0.02° and a step time of 1 s. The final diffraction plot with the difference between the observed and calculated profiles of $BaMo_2O_5(SeO_3)_2$ has been deposited as Supporting Information.

IR Spectroscopy. IR spectra were recorded on a Varian 1000 Fourier transform IR spectrometer in the 400−4000 cm^{-1} range, with

Table 1. Crystallographic Data for $SrMo_2O_5(SeO_3)_2$ and $PbMo_2O_5(SeO_3)_2$

formula	$SrMo_2Se_2O_{11}$	$PbMo_2Se_2O_{11}$
fw	613.42	732.99
space group	$P\bar{1}$ (No. 2)	$P\bar{1}$ (No. 2)
a (Å)	7.8759(6)	7.8560(6)
b (Å)	8.1509(5)	8.2307(6)
c (Å)	8.8076(6)	8.8381(6)
α (deg)	82.943(5)	82.881(4)
β (deg)	65.326(5)	64.843(4)
γ (deg)	66.918(5)	66.419(4)
V (Å^3)	472.09(6)	473.34(6)
Z	2	2
T (°C)	200.0(2)	200.0(2)
λ (Å)	0.71073	0.71073
ρ_{calcd} (g cm^{-3})	4.315	5.143
μ (mm^{-1})	16.004	28.089
$R(F)^a$	0.0522	0.0566
$R_w(F_o^2)^b$	0.1155	0.1452

$^aR(F) = \sum||F_o| - |F_c||/\sum|F_o|$. $^bR_w(F_o^2) = [\sum w(F_o^2 - F_c^2)^2/\sum w(F_o^2)^2]^{1/2}$.

Table 2. Selected Bond Distances (Å) for $SrMo_2O_5(SeO_3)_2$ and $PbMo_2O_5(SeO_3)_2$

$SrMo_2O_5(SeO_3)_2$		$PbMo_2O_5(SeO_3)_2$	
Mo(1)−O(1)	1.704(8)	Mo(1)−O(1)	1.694(13)
Mo(1)−O(2)	1.714(8)	Mo(1)−O(2)	1.722(12)
Mo(1)−O(3)	1.877(8)	Mo(1)−O(3)	1.873(12)
Mo(1)−O(4)	2.091(8)	Mo(1)−O(4)	2.089(12)
Mo(1)−O(5)	2.170(8)	Mo(1)−O(5)	2.135(13)
Mo(1)−O(5)	2.326(7)	Mo(1)−O(5)	2.347(12)
Mo(2)−O(3)	1.866(8)	Mo(2)−O(3)	1.878(12)
Mo(2)−O(6)	1.710(8)	Mo(2)−O(6)	1.694(14)
Mo(2)−O(7)	1.706(7)	Mo(2)−O(7)	1.718(12)
Mo(2)−O(8)	2.060(7)	Mo(2)−O(8)	2.082(12)
Mo(2)−O(9)	2.179(8)	Mo(2)−O(9)	2.174(13)
Mo(2)−O(9)	2.278(8)	Mo(2)−O(9)	2.321(11)
Se(1)−O(5)	1.734(8)	Se(1)−O(5)	1.759(11)
Se(1)−O(8)	1.737(7)	Se(1)−O(8)	1.723(11)
Se(1)−O(10)	1.646(8)	Se(1)−O(10)	1.647(12)
Se(2)−O(4)	1.710(8)	Se(2)−O(4)	1.706(12)
Se(2)−O(9)	1.751(7)	Se(2)−O(9)	1.725(13)
Se(2)−O(11)	1.649(8)	Se(2)−O(11)	1.641(11)
Sr(1)−O(2)	2.599(8)	Pb(1)−O(2)	2.675(11)
Sr(1)−O(4)	2.692(8)	Pb(1)−O(4)	2.750(11)
Sr(1)−O(7)	2.547(7)	Pb(1)−O(7)	2.604(12)
Sr(1)−O(8)	2.665(8)	Pb(1)−O(8)	2.708(12)
Sr(1)−O(10)	2.531(8)	Pb(1)−O(10)	2.552(13)
Sr(1)−O(10)	2.586(8)	Pb(1)−O(10)	2.588(13)
Sr(1)−O(11)	2.540(8)	Pb(1)−O(11)	2.633(12)
Sr(1)−O(11)	2.676(8)	Pb(1)−O(11)	2.637(12)

dx.doi.org/10.1021/ic3003564 | *Inorg. Chem.* 2012, 51, 5393−5399

the sample embedded in a KBr matrix. IR ($SrMo_2O_5(SeO_3)_2$, cm^{-1}): 950 (m), 936 (m), 922 (m), 901 (s), 862 (s), 817 (m), 726 (s, br), 620 (s, br), 571 (m), 535 (m), 473 (m). IR ($PbMo_2O_5(SeO_3)_2$, cm^{-1}): 944 (m), 931 (m), 912 (m), 892 (s), 840 (m), 826 (m), 806 (m), 720 (s, br), 646 (m, sh), 617 (s), 560 (m), 518 (m), 463 (m).

Thermogravimetric Analysis. Thermogravimetric analysis was performed on a Setaram LABSYS TG-DTA/DSC thermogravimetric analyzer. The polycrystalline samples were contained within alumina crucibles and heated at a rate of 10 °C min^{-1} from room temperature to 800 °C under flowing argon.

Scanning Electron Microscopy/Energy-Dispersive Analysis by X-ray (SEM/EDAX). SEM/EDAX has been performed using a Hitachi S-3400N/Horiba Energy EX-250 instrument. EDAX for $SrMo_2O_5(SeO_3)_2$ and $PbMo_2O_5(SeO_3)_2$ exhibits Sr:Mo:Se and Pb:Mo:Se ratios of approximately 1:2:2.

Second-Order NLO Measurements. Powder SHG measurements on polycrystalline $BaMo_2O_5(SeO_3)_2$ were performed on a modified Kurtz-NLO system[40] using 1064 nm radiation. A DAWA Q-switched Nd:YAG laser, operating at 20 Hz, was used for the measurements. Because SHG efficiency has been shown to depend strongly on the particle size; polycrystalline samples were ground and sieved (Newark Wire Cloth Co.) into distinct particle size ranges (20–45, 45–63, 63–75, 75–90, 90–125, and >125 μm). To make relevant comparisons with known SHG materials, crystalline α-SiO_2 and $LiNbO_3$ were also ground and sieved into the same particle size ranges. Powders with particle size 45–63 μm were used for comparing SHG intensities. All of the powder samples with different particle sizes were placed in separate capillary tubes. No index-matching fluid was used in any of the experiments. The SHG light, i.e., 532 nm green light, was collected in reflection and detected by a photomultiplier tube (Hamamatsu). To detect only the SHG light, a 532 nm narrow-pass interference filter was attached to the tube. A digital oscilloscope (Tektronix TDS1032) was used to view the SHG signal. A detailed description of the equipment and methodology used has been published.[41]

RESULTS AND DISCUSSION

Structures. $SrMo_2O_5(SeO_3)_2$ and $PbMo_2O_5(SeO_3)_2$ are isostructual and crystallize in the CS space group $P\bar{1}$ (No. 2). The materials are new quaternary mixed-metal selenites exhibiting chain structures with distorted MoO_6 octahedra linked by asymmetric SeO_3 polyhedra (see Figure 1). There are two unique Mo^{6+} cations within an asymmetric unit. Both Mo^{6+} cations are in highly distorted octahedral coordination environments with six O atoms attributable to the SOJT distortions. Especially, the two unique Mo^{6+} cations distort along the local C_3 [111] direction, toward a face, of their respective octahedra (see Figure 2a). The out-of-center distortions result in three short [1.704(8) to 1.877(8) Å for $SrMo_2O_5(SeO_3)_2$ and 1.694(13)–1.878(12) Å for $PbMo_2O_5(SeO_3)_2$] and three long [2.060(7)–2.326(7) Å for $SrMo_2O_5(SeO_3)_2$ and 2.082(12)–2.347(12) Å for $PbMo_2O_5(SeO_3)_2$] Mo–O bond distances. The two unique Se^{4+} cations are in distorted trigonal-pyramidal environments, bonded to three O atoms (see Figure 2b). The Se–O bond lengths range from 1.646(8) to 1.751(7) Å for $SrMo_2O_5(SeO_3)_2$ and from 1.641(11) to 1.759(11) Å for $PbMo_2O_5(SeO_3)_2$. The Se^{4+} cations are in asymmetric coordination environments attributable to the stereoactive lone pair. Finally, each unique Sr^{2+} or Pb^{2+} cation exhibits an eight-coordinate square-antiprismatic environment, with Sr–O or Pb–O contact distances ranging from 2.531(8) to 2.692(8) Å and from 2.552(13) to 2.750(11) Å for $SrMo_2O_5(SeO_3)_2$ and $PbMo_2O_5(SeO_3)_2$, respectively.

As can be seen in Figure 3a, the backbone of the structure may be described as zigzag chains of edge- and corner-shared

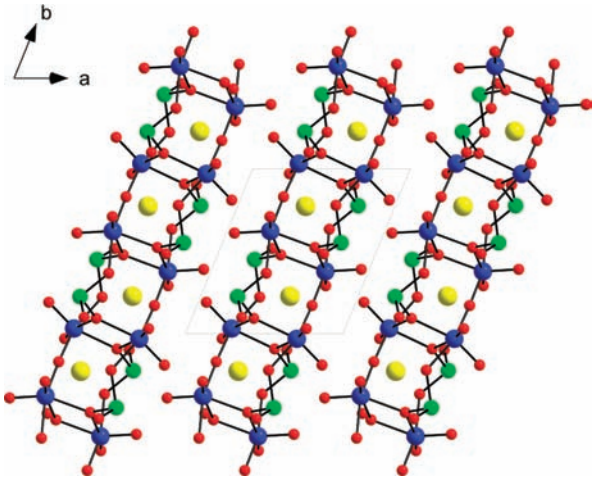

Figure 1. Ball-and-stick representation of $SrMo_2O_5(SeO_3)_2$ in the *ab* plane. The distorted MoO_6 octahedra and asymmetric SeO_3 polyhedra link to form chains along the [010] direction (blue, Mo; green, Se; yellow, Sr; red, O).

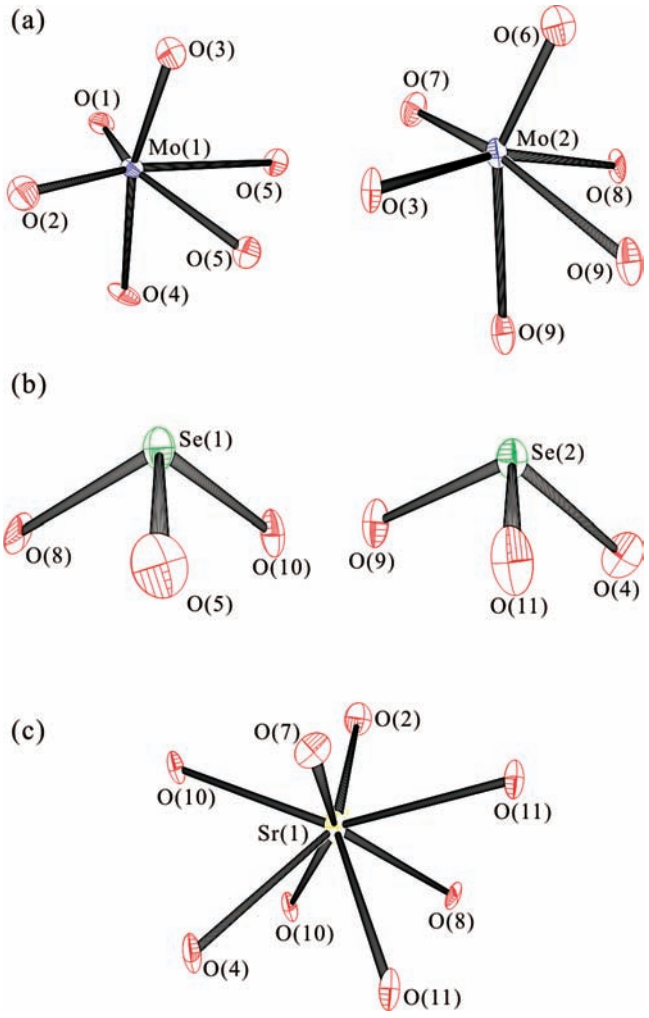

Figure 2. ORTEP (50% probability ellipsoids) representations in $SrMo_2O_5(SeO_3)_2$ showing (a) the MoO_6 octahedra with C_3 out-of-center distortions, (b) the asymmetric SeO_3 polyhedra, and (c) the SrO_8 polyhedra.

dx.doi.org/10.1021/ic3003564 | Inorg. Chem. 2012, 51, 5393–5399

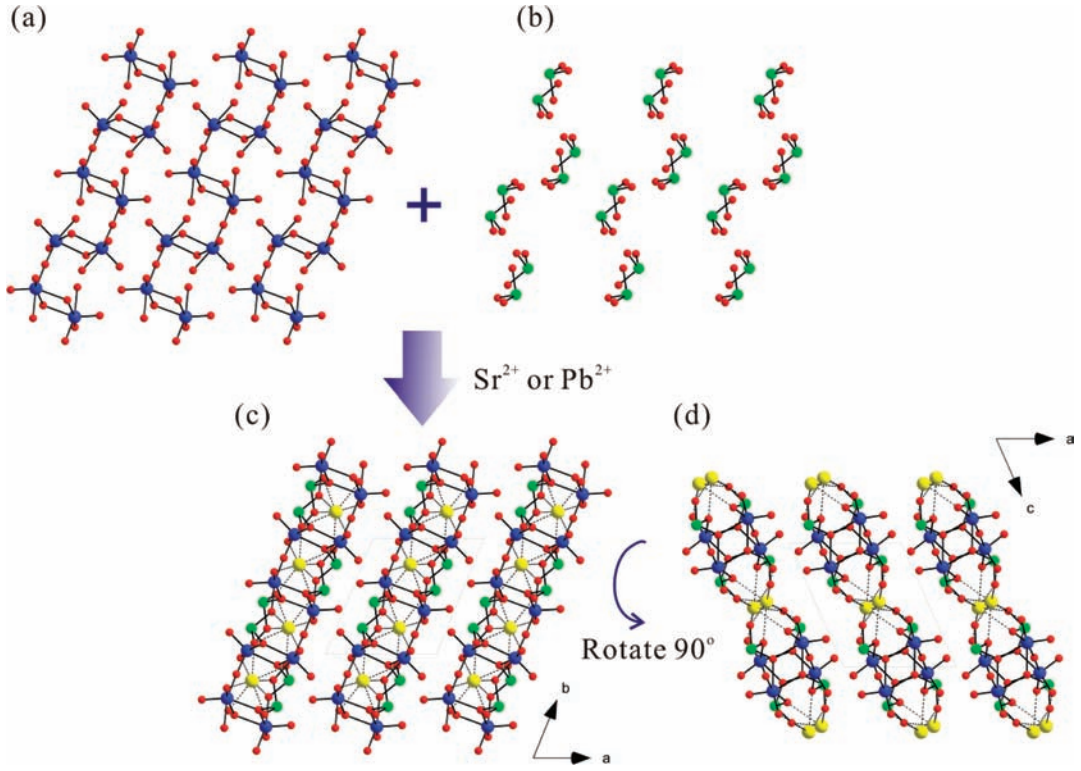

Figure 3. Ball-and-stick models of $SrMo_2O_5(SeO_3)_2$ representing (a) zigzag chains of edge- and corner-shared MoO_6 octahedra running along the [010] direction, (b) SeO_3 polyhedra, and (c) the "linking" of the chains by SeO_3 and SrO_8 groups. (d) Note that a pseudo-two-dimensional topology is observed in the *ac* plane attributable to the Sr−O contacts (blue, Mo; green, Se; yellow, Sr; red, O).

MoO_6 octahedra. Two $Mo(1)O_6$ octahedra share their edges through O(5) and form a $Mo(1)_2O_{10}$ dimer. Also, two $Mo(2)O_6$ octahedra share their edges through O(9) and form another $Mo(2)_2O_{10}$ dimer. Then the $Mo(1)_2O_{10}$ and $Mo(2)_2O_{10}$ dimers share their corners through O(3) and form infinite zigzag chains along the [010] direction. Then, the chains are capped by the SeO_3 groups along the [100] and [−100] directions (see Figure 3b). Interestingly, all SeO_3 groups serve as intrachain linkers. Finally, interchain Sr−O (or Pb−O) contacts are observed in the *ac* plane (see the dashed lines in Figure 3c,d). The interchain contacts might give $SrMo_2O_5(SeO_3)_2$ and $PbMo_2O_5(SeO_3)_2$ a pseudo-two-dimensional topology. In connectivity terms, the structures of $SrMo_2O_5(SeO_3)_2$ and $PbMo_2O_5(SeO_3)_2$ may be described as anionic chains of $\{[Mo(1)_2O_{4/1}O_{4/2}O_{2/3}]^{-1.333}[Mo(2)_2O_{4/1}O_{4/2}O_{2/3}]^{-1.333}[Se(1)O_{1/1}O_{1/2}O_{1/3}]^{+0.333}[Se(2)O_{1/1}O_{1/2}O_{1/3}]^{+0.333}\}^{-2}$. The charge balance is maintained by incorporation of the Sr^{2+} or Pb^{2+} cations. Bond-valence-sum calculations[42,43] for the Mo^{6+}, Se^{4+}, and Sr^{2+} (or Pb^{2+}) result in values in the ranges 5.92−6.05, 3.98−4.17, and 2.18 (or 1.93), respectively.

IR Spectroscopy. The IR spectra of $SrMo_2O_5(SeO_3)_2$ and $PbMo_2O_5(SeO_3)_2$ revealed overlapped bands of Mo−O, Se−O, Pb−O, and Sr−O vibrations below 1000 cm^{-1}. The Mo−O and Se−O vibrations are only partially resolved as previously reported.[24,27] Also, no vibrational bands are observed between 4000 and 1000 cm^{-1}, which is consistent with similar materials. The IR spectra for the reported materials have been deposited as Supporting Information.

Thermal Analysis. The thermal behaviors of the reported materials were investigated using thermogravimetric analysis and powder XRD measured at different temperatures. As indicated by the thermogravimetric analysis diagram, $PbMo_2O_5(SeO_3)_2$ is stable up to 400 °C. Above the temperature, decompositions occur attributable to the sublimation of SeO_2. The thermal stabilities of $SrMo_2O_5(SeO_3)_2$ and $PbMo_2O_5(SeO_3)_2$ were also confirmed by powder XRD. As can be seen in the Supporting Information, no substantial changes in the peak position and intensity are observed in the XRD patterns up to 400 °C. However, the XRD patterns obtained at higher temperatures revealed that the materials decomposed to the mixture of $SrMoO_4$ (PDF#08-0482) and MoO_3 (PDF#05-0508) or $PbMoO_4$ (PDF#44-1486) and MoO_3 (PDF#05-0508).

Second-Order NLO Measurements. Although the structure of NCS $BaMo_2O_5(SeO_3)_2$ has been published,[27] the NLO properties of the material have not been studied yet. Thus, we investigated its NLO properties. Powder SHG measurements, using 1064 nm radiation, indicated that $BaMo_2O_5(SeO_3)_2$ has a SHG efficiency of approximately 80 times that of α-SiO_2. By sieving $BaMo_2O_5(SeO_3)_2$ powder into various particle sizes, ranging from 20 to 150 μm, and measuring the SHG as a function of the particle size, we were able to determine the type 1 phase-matching capabilities of the material. As seen in Figure 4, $BaMo_2O_5(SeO_3)_2$ is phase-matchable. Once the SHG efficiency and the phase-matching capability of a material are known, the bulk SHG efficiency, $\langle d_{eff}\rangle_{exp}$, can be estimated.[44] For $BaMo_2O_5(SeO_3)_2$, $\langle d_{eff}\rangle_{exp}$ is approximately 10.3 pm V^{-1}.

Structure−Property Relationships. The observed SHG response can be understood by analyzing the polarization of the asymmetric polyhedra. Specifically, macroscopic NCS is normally observed when locally polar asymmetric coordination polyhedra add constructively. Thus, it is crucial to determine

dx.doi.org/10.1021/ic3003564 | *Inorg. Chem.* 2012, 51, 5393−5399

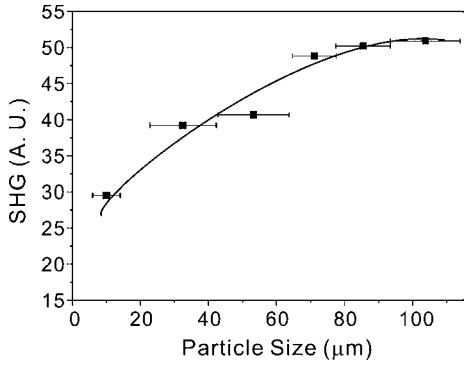

Figure 4. Phase-matching curve (type 1) for $BaMo_2O_5(SeO_3)_2$. The curve is to guide the eye and is not a fit to the data.

the "net" direction of the polarizations, in which the origin and magnitude of the SHG properties can be obtained. In $BaMo_2O_5(SeO_3)_2$, both kinds of SOJT-distortive cations, Mo^{6+} and Se^{4+} may significantly contribute toward the SHG efficiency. First, the Mo^{6+} cations distort either along the [011] or [0−11] directions, resulting in two short, two normal, and two long Mo−O bonds. Once taken as a whole, a net moment is observed pointing in the [001] direction (see Figure 5).

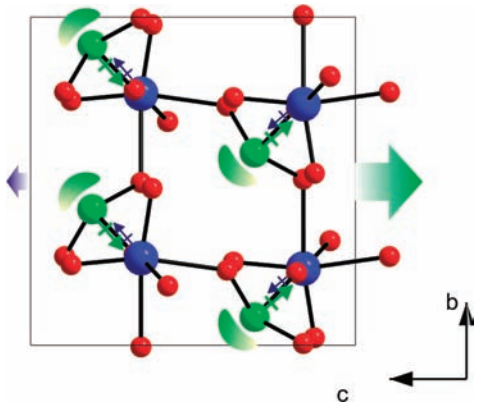

Figure 5. Ball-and-stick representation of $BaMo_2O_5(SeO_3)_2$ (blue, Mo; green, Se; red, O). A moment is observed toward the [001] direction attributable to the alignment of the C_2 out-of-center distorted MoO_6 octahedra. Also, a larger net moment attributed to the sum of the aligned asymmetric SeO_3 groups is observed in the [00−1] direction. Once taken as a whole, a net moment is observed along the [00−1] direction.

Meanwhile, each SeO_3 unit also has a dipole moment attributable to the different charge distributions on Se and O atoms. As seen in Figure 5, the lone pairs on the asymmetric Se^{4+} cations approximately point toward the [011] and [0−11] directions. Because the local moment for SeO_3 points in the opposite direction of the lone pair, a net moment in the [00−1] direction attributable to the alignment of lone pairs on Se^{4+} cations is observed (see Figure 5). At this point, one can notice that the moments for MoO_6 octahedra and SeO_3 polyhedra point in opposite directions. As we will discuss later, the local dipole moment calculations indicate that the moment for SeO_3 is larger than that of the MoO_6 octahedra. Thus, taking the moments as a whole, a net moment is observed along the [00−1] direction. This net moment that is mainly arising from the alignment of asymmetric SeO_3 groups is responsible for the observed moderate SHG response, 80 times that of α-SiO_2.

In order to better understand the asymmetric coordination environment and the macroscopic net polarization, we did calculate the local dipole moments for Mo^{6+} and Se^{4+} in $AMo_2O_5(SeO_3)_2$ (A = Sr, Pb, and Ba). This approach has been described earlier with respect to metal oxyfluoride octahedra.[45,46] We found that the local dipole moments for the SeO_3 polyhedra in the reported materials range about from 8.00 to 8.73 D, respectively. The values are consistent with the recently reported dipole moments for SeO_3 polyhedra.[47] Also, the local dipole moments for the four MoO_6 octahedra exhibit values ranging from 4.56 to 5.98 D. Especially with $BaMo_2O_5(SeO_3)_2$, the local dipole moments for SeO_3 and MoO_6 were calculated to be 8.73 and 4.56, respectively. A complete calculation of dipole moments for the constituted polyhedra is listed in Table 3.

Table 3. Calculation of Dipole Moments for SeO_3 and MoO_6 Polyhedra

compound	species	dipole moment (D)
$SrMo_2O_5(SeO_3)_2$	$Se(1)O_3$	8.17
	$Se(2)O_3$	8.00
	$Mo(1)O_6$	5.33
	$Mo(2)O_6$	4.99
$PbMo_2O_5(SeO_3)_2$	$Se(1)O_3$	8.13
	$Se(2)O_3$	8.49
	$Mo(1)O_6$	5.98
	$Mo(2)O_6$	5.36
$BaMo_2O_5(SeO_3)_2$	$Se(1)O_3$	8.73
	$Mo(1)O_6$	4.56

CS Nonpolar versus NCS Polar Structures. Although $SrMo_2O_5(SeO_3)_2$, $PbMo_2O_5(SeO_3)_2$, and $BaMo_2O_5(SeO_3)_2$ are stoichiometrically equivalent, an interesting change in the crystallographic polarity occurs from the CS nonpolar structure for the materials containing relatively smaller cations, Sr^{2+} or Pb^{2+}, to the NCS polar structure for that with the larger one, Ba^{2+}. While $SrMo_2O_5(SeO_3)_2$ or $PbMo_2O_5(SeO_3)_2$ exhibits a CS pseudo-two-dimensional-layered structure, $BaMo_2O_5(SeO_3)_2$ shows a NCS three-dimensional framework. With $SrMo_2O_5(SeO_3)_2$ or $PbMo_2O_5(SeO_3)_2$, the Sr^{2+} or Pb^{2+} cation is in an eight-coordinate square-antiprismatic environment. However, the Ba^{2+} cation in $BaMo_2O_5(SeO_3)_2$ possesses a 10-coordinate geometry. The different coordination environments are consistent with the ionic radii of the cations (Sr^{2+}, 1.26 Å; Pb^{2+}, 1.29 Å; Ba^{2+}, 1.42 Å).[48] Relatively smaller cations, Sr^{2+} or Pb^{2+}, interact with oxide ligands on four MoO_6 octahedra and four SeO_3 polyhedra (see Figure 6a). As seen in Figure 6a, in order to maintain the crowded eight-coordinate square-antiprismatic environment around the Sr^{2+} or Pb^{2+} cation, the MoO_6 octahedra and SeO_3 polyhedra are coordinated in an antiparallel manner. By doing so, any unfavorable repulsion of polyhedra can be minimized. In other words, the Sr^{2+} or Pb^{2+} cation serves as an inversion center, which renders the material CS nonpolar. In $BaMo_2O_5(SeO_3)_2$, a 10-fold coordination environment is observed, attributable to the large ionic size of Ba^{2+} (see Figure 6b). The larger cation, Ba^{2+}, can interact with oxide ligands on eight MoO_6 octahedra and two SeO_3 groups. More specifically, four pairs of corner-sharing MoO_6 octahedra; i.e., Mo_2O_{11} groups completely encompass the Ba^{2+} cation. Then the only way to assert the 10-coordinate environment in the Ba^{2+} cation with two more SeO_3 groups is to connect Se^{4+} cations to O(4) and O(6) [the

dx.doi.org/10.1021/ic3003564 | Inorg. Chem. 2012, 51, 5393−5399

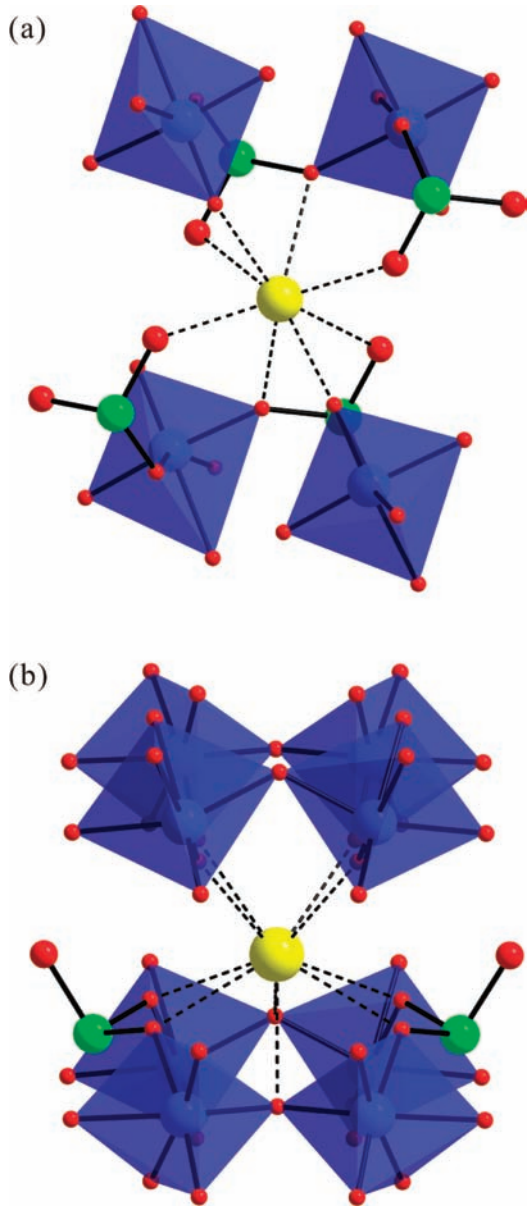

Figure 6. Ball-and-stick and polyhedral representations of (a) $SrMo_2O_5(SeO_3)_2$ and (b) $BaMo_2O_5(SeO_3)_2$ (blue, Mo; green, Se; red, O). With $SrMo_2O_5(SeO_3)_2$, the MoO_6 octahedra and SeO_3 polyhedra are coordinated in an antiparallel manner to maintain the eight-coordinate square-antiprismatic environment around the Sr^{2+} cation. For $BaMo_2O_5(SeO_3)_2$, Mo_2O_{11} groups completely encompass the Ba^{2+} cation; thus, the two SeO_3 groups are connected in a parallel manner to assert the 10-coordinate environment around the Ba^{2+} cation.

O(4)−O(6) contact is 2.541(9) Å], which spontaneously results in a parallel alignment of lone pairs. All of the other O−O contacts observed around the Ba^{2+} cation are too long for the connection of SeO_3 groups. This parallel alignment of SeO_3 polyhedra results in a NCS polar material. The similar cation size effect on the coordination environments of framework polyhedra and subsequent overall centricity have been observed before from a series of stoichiometrically equivalent mixed-metal oxides.[19,20,24−26,28] In other words, local asymmetric environments normally observed from SOJT cations can be controlled by other factors to increase the incidence of crystallographic NCS. Here the size of the A-site cations is a major factor in determining the space group centricities.

CONCLUSIONS

We have successfully synthesized stoichiometrically equivalent mixed-metal selenite materials, $AMo_2O_5(SeO_3)_2$ (A = Sr, Pb, and Ba), by standard solid-state reactions. Crystallographic data indicate that $SrMo_2O_5(SeO_3)_2$ and $PbMo_2O_5(SeO_3)_2$ are CS nonpolar with pseudo-two-dimensional structures, whereas $BaMo_2O_5(SeO_3)_2$ is NCS polar with a three-dimensional framework structure. Detailed structural analyses suggest that the cation size and coordination number play critical roles to determine the symmetry and framework of the materials. Powder SHG measurements on $BaMo_2O_5(SeO_3)_2$ using 1064 nm radiation indicate that the material is phase-matchable (type 1) with a SHG efficiency of approximately 80 times that of α-SiO_2. We are in the process of synthesizing other new NCS mixed-metal oxide materials and will be reporting on them shortly.

ASSOCIATED CONTENT

Supporting Information

X-ray crystallographic file in CIF format, calculated and observed XRD patterns, thermal analysis diagrams, and IR spectra for $AMo_2O_5(SeO_3)_2$. This material is available free of charge via the Internet at http://pubs.acs.org.

AUTHOR INFORMATION

Corresponding Author

*E-mail: kmok@cau.ac.kr. Phone: +82-2-820-5197 Fax: +82-2-825-4736.

Notes

The authors declare no competing financial interest.

ACKNOWLEDGMENTS

This research was supported by Basic Science Research Program through the National Research Foundation of Korea (NRF) funded by Ministry of Education, Science & Technology (Grant 2010-0002480).

REFERENCES

(1) Jona, F.; Shirane, G. *Ferroelectric Crystals*; Pergamon Press: Oxford, U.K., 1962.
(2) Cady, W. G. *Piezoelectricity; an Introduction to the Theory and Applications of Electromechanical Phenomena in Crystals*; Dover: New York, 1964; p 822.
(3) Lang, S. B. *Sourcebook of Pyroelectricity*; Gordon & Breach Science: London, 1974.
(4) Galy, J.; Meunier, G. *J. Solid State Chem.* **1975**, *13*, 142.
(5) Auciello, O.; Scott, J. F.; Ramesh, R. *Phys. Today* **1998**, *40*, 22.
(6) Valasek, J. *Phys. Rev.* **1920**, *15*, 537.
(7) Franken, P. A.; Hill, A. E.; Peters, C. W.; Weinreich, G. *Phys. Rev. Lett.* **1961**, *7*, 118.
(8) Halasyamani, P. S.; Poeppelmeier, K. R. *Chem. Mater.* **1998**, *10*, 2753.
(9) Opik, U.; Pryce, M. H. L. *Proc. R. Soc. London* **1957**, *A238*, 425.
(10) Bader, R. F. W. *Mol. Phys.* **1960**, *3*, 137.
(11) Pearson, R. G. *J. Mol. Struct.: THEOCHEM* **1983**, *103*, 25.
(12) Wheeler, R. A.; Whangbo, M.-H.; Hughbanks, T.; Hoffmann, R.; Burdett, J. K.; Albright, T. A. *J. Am. Chem. Soc.* **1986**, *108*, 2222.
(13) Pan, S.; Smit, J. P.; Watkins, B.; Marvel, M. R.; Stern, C. L.; Poeppelmeier, K. R. *J. Am. Chem. Soc.* **2006**, *128*, 11631.
(14) Inaguma, Y.; Yoshida, M.; Katsumata, T. *J. Am. Chem. Soc.* **2008**, *130*, 6704.

(15) Kepert, C. J.; Prior, T. J.; Rosseinsky, M. J. *J. Am. Chem. Soc.* **2000**, *122*, 5158.
(16) Maggard, P. A.; Stern, C. L.; Poeppelmeier, K. R. *J. Am. Chem. Soc.* **2001**, *123*, 7742.
(17) Hwu, S.-J.; Ulutagay-Kartin, M.; Clayhold, J. A.; Mackay, R.; Wardojo, T. A.; O'Connor, C. J.; Kraweic, M. *J. Am. Chem. Soc.* **2002**, *124*, 12404.
(18) Welk, M. E.; Norquist, A. J.; Arnold, F. P.; Stern, C. L.; Poeppelmeier, K. R. *Inorg. Chem.* **2002**, *41*, 5119.
(19) Sykora, R. E.; Ok, K. M.; Halasyamani, P. S.; Albrecht-Schmitt, T. E. *J. Am .Chem. Soc.* **2002**, *124*, 1951.
(20) Goodey, J.; Ok, K. M.; Broussard, J.; Hofmann, C.; Escobedo, F. V.; Halasyamani, P. S. *J. Solid State Chem.* **2003**, *175*, 3.
(21) Ok, K. M.; Baek, J.; Halasyamani, P. S.; O'Hare, D. *Inorg. Chem.* **2006**, *45*, 10207.
(22) Choi, M.-H.; Kim, S.-H.; Chang, H. Y.; Halasyamani, P. S.; Ok, K. M. *Inorg. Chem.* **2009**, *48*, 8376.
(23) Halasyamani, P. S. *Chem. Mater.* **2004**, *16*, 3586.
(24) Harrison, W. T. A.; Dussack, L. L.; Jacobson, A. J. *Inorg. Chem.* **1994**, *33*, 6043.
(25) Ling, J.; Albrecht Schmitt, T. E. *J. Solid State Chem.* **2007**, *180*, 1601.
(26) Chang, H. Y.; Kim, S. W.; Halasyamani, P. S. *Chem. Mater.* **2010**, *22*, 3241.
(27) Harrison, W. T. A.; Dussack, L. L.; Jacobson, A. J. *J. Solid State Chem.* **1996**, *125*, 234.
(28) Porter, Y.; Halasyamani, P. S. *J. Solid State Chem.* **2003**, *174*, 441.
(29) Shen, Y. L.; Jiang, H. L.; Xu, J.; Mao, J. G.; Cheah, K. W. *Inorg. Chem.* **2005**, *44*, 9314.
(30) Kong, F.; Hu, C.; Hu, T.; Zhou, Y.; Mao, J. G. *Dalton Trans.* **2009**, *2009*, 4962.
(31) Li, P.; Hu, C.; Xu, X.; Wang, R.; Sun, C. F.; Mao, J.-G. *Inorg. Chem.* **2010**, *49*, 4599.
(32) Jiang, H.; Xie, Z.; Mao, J. G. *Inorg. Chem.* **2007**, *46*, 6495.
(33) Zhang, S.; Jiang, H.; Sun, C.; Mao, J. G. *Inorg. Chem.* **2009**, *48*, 11809.
(34) *SAINT, Program for Area Detector Absorption Correction*; version 4.05; Siemens Analytical X-ray Instruments: Madison, WI, 1995.
(35) Blessing, R. H. *Acta Crystallogr., Sect. A: Found. Crystallogr.* **1995**, *A51*, 33.
(36) Sheldrick, G. M. *SHELXS-97—A program for automatic solution of crystal structures*; University of Goettingen: Goettingen, Germany, 1997.
(37) Sheldrick, G. M. *SHELXL-97—A program for crystal structure refinement*; University of Goettingen: Goettingen, Germany, 1997.
(38) Farrugia, L. J. *J. Appl. Crystallogr.* **1999**, *32*, 837.
(39) Larson, A. C.; von Dreele, R. B. *General Structural Analysis System (GSAS)*; Los Alamos National Laboratory: Los Alamos, NM, 1987.
(40) Kurtz, S. K.; Perry, T. T. *J. Appl. Phys.* **1968**, *39*, 3798.
(41) Ok, K. M.; Chi, E. O.; Halasyamani, P. S. *Chem. Soc. Rev.* **2006**, *35*, 710.
(42) Brown, I. D.; Altermatt, D. *Acta Crystallogr.* **1985**, *B41*, 244.
(43) Brese, N. E.; O'Keeffe, M. *Acta Crystallogr.* **1991**, *B47*, 192.
(44) Goodey, J.; Broussard, J.; Halasyamani, P. S. *Chem. Mater.* **2002**, *14*, 3174.
(45) Maggard, P. A.; Nault, T. S.; Stern, C. L.; Poeppelmeier, K. R. *J. Solid State Chem.* **2003**, *175*, 25.
(46) Izumi, H. K.; Kirsch, J. E.; Stern, C. L.; Poeppelmeier, K. R. *Inorg. Chem.* **2005**, *44*, 884.
(47) Lee, D. W.; Ok, K. M. *Solid State Sci.* **2010**, *12*, 2036.
(48) Shannon, R. D. *Acta Crystallogr.* **1976**, *A32*, 751.